Phase behavior of disk-coil block copolymers under cylindrical confinement: Curvature-induced structural frustrations

Min Young Ha,[1,*] Ji Ho Ryu,[1,*] Eugene N. Cho,[2] Junwon Choi,[3,4] YongJoo Kim,[2,†] and Won Bo Lee[1,‡]

[1]*School of Chemical and Biological Engineering, Institute of Chemical Processes, Seoul National University, Seoul 08826, Republic of Korea*

[2]*KAIST Institute for NanoCentury, Korea Advanced Institute of Science and Technology (KAIST), Daejeon 34141, Republic of Korea*

[3]*Chemical Kinomics Research Center, Korea Institute of Science and Technology (KIST), Seoul 02792, Republic of Korea*

[4]*Bio-Med Division, KIST-School UST, Seoul 02792, Republic of Korea*

(Received 14 June 2019; published 15 November 2019)

In this paper, we explore the self-assembly behavior of disk-coil block copolymers (BCPs) confined within a cylinder using molecular dynamics simulations. As functions of the diameter of the confining cylinder and the number of coil beads, concentric lamellar structures are obtained with a different number of alternating disk-rich and coil-rich bilayers. Our paper focuses on the curvature-induced structural behavior in the disk-rich domain of a self-assembled structure, which is investigated by calculating the local density distribution $P(r)$ and the orientational distribution $G(r,\theta)$. In the inner layers of cylinder-confined disk-coil BCPs, both $P(r)$ and $G(r,\theta)$ show characteristic asymmetry within a bilayer which is directly contrasted with the bulk and slab-confined disk-coil BCPs. We successfully explain the structural frustration of disks arising from the curved structure due to packing frustration of disks and asymmetric stretching of coils to the regions with different curvatures in a bilayer. Our results are important to understand the self-assembly behavior of BCPs containing a rigid motif in a confined structure, such as a self-assembled structure of bacteriochlorophyll molecules confined by a lipid layer to form a chlorosome, the photosynthetic antennae complex found in nature.

DOI: 10.1103/PhysRevE.100.052502

I. INTRODUCTION

Phase behavior of block copolymers (BCPs) has been intensively studied over the past decades from both experimental and theoretical perspectives for developing next-generation nanoscale patterning technology [1–6]. It is now well understood that balancing the enthalpy from the interface between the different blocks and the stretching energy from chain entropy leads to a rich phase behavior of the BCPs, allowing diverse nanostructures, such as disordered, lamellar, cylindrical, spherical, and bicontinuous gyroid phases depending on the segregation strength and relative volume fraction between the different blocks [7–10]. The phase behavior of BCPs can be greatly modified by introducing a block with different molecular shape and rigidity. Representative cases are the rod-coil [11–15] and disk-coil BCPs [16–18] where one of the blocks has rigid molecular shapes resembling rodlike or discotic liquid crystals, respectively. Rigid blocks of these copolymers share general characteristics with liquid crystalline molecules, such as the orientational ordering tendency to align with its neighbors that results in nematic or smectic phases within the microphase separated layers [19–21]. As a result, the thermodynamically stable structures of the rod-coil and the disk-coil BCPs are distinct from those of traditional coil-coil BCPs and exhibit a qualitatively different phase diagram.

Another interesting aspect of BCP phase behavior can be realized by placing the BCP in spatial confinement. Previously, intensive studies were performed on the phase behavior when confining the BCPs in slabs [22–24], cylinders [25–31], and spheres [32,33], both experimentally and theoretically. Phase behavior in these systems strongly depends on the wall-polymer interactions and the ratio between the relative size of the confinement and characteristic length of BCPs, highlighting the influence of structural frustrations induced by the confining walls. Especially, cylindrically confined BCPs can be self-assembled into more complex three-dimensional structures, such as helices and stacked toroids for designing photonic crystals and optoelectronic devices [25,26]. In this perspective, a natural question arises on the phase behavior of rod-coil and disk-coil BCPs in cylindrical confinement. Since the rigid blocks have very low stretchability due to the intermolecular interactions, such as π-π stacking, rearrangement of the rigid block in the curved environment is relatively difficult compared to the coil-coil BCPs. Moreover, in cylindrical confinement, perfect stacking of the rods or disks may not be preferred due to the curved environment, and the cavity induced by imperfect stacking leads to further deviation of the phase behavior from its bulk counterpart. The effect of these spatial frustrations on the thermodynamics of the confined BCPs with shape asymmetric rigid blocks is not a trivial matter to address, and intensive research is required to explore their phase behavior. There has been a recent report of cylindrically confined rod-coil BCPs by using dissipative particle dynamics simulation [34], however, studies on confined disk-coil BCPs have gained less attention despite its theoretical importance.

The study on the disk-coil BCPs has also practical implications apart from theoretical interest due to the abundant

*These authors contributed equally to this paper.

†cjyjee@kaist.ac.kr

‡wblee@snu.ac.kr

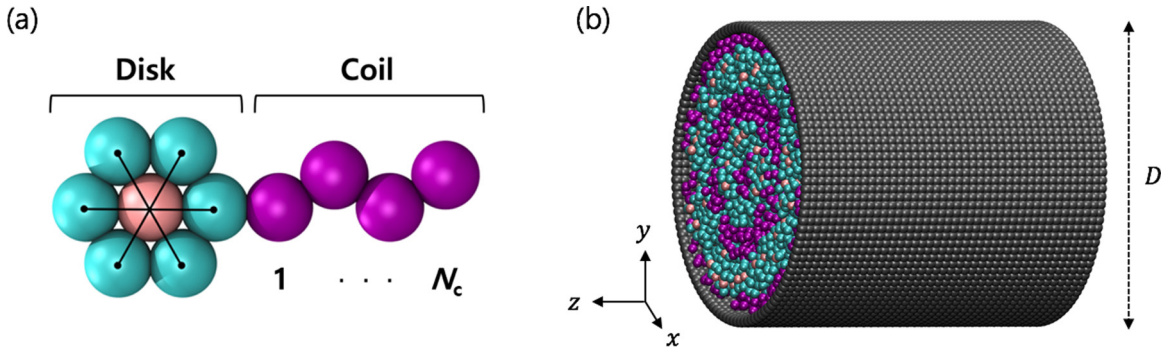

FIG. 1. (a) Modeled disk-coil BCPs. The blue beads represent the peripheral beads of the disk block, and the purple beads represent the coil block. The central bead of the disk block is highlighted in pink. The black lines show three extra harmonic springs, introduced for the rigidity of the disk. (b) Simulated disk-coil BCPs within cylindrical wall with diameter D composed of gray beads.

disk-coil motifs that can be found in light-harvesting complexes in nature [35,36]. Chlorophyll, the light-harvesting pigment universally found in green plants, is composed of a chlorin- or porphyrinlike disk functionalized by a single alkyl chain. Of special interest is the bacteriochlorophyll (Bchl) molecules utilized by phototrophic bacteria living in extremely low-light environments. Bchl molecules self-assemble into chlorosome, a large light-harvesting antennae complex, that allows bacteria to collect energy even in low-light environments in a highly efficient way [37–39]. It is now generally accepted that the self-assembly of Bchl is guided mostly by Bchl-Bchl interactions and geometrical requirements of confining membranes, whereas chlorophyll in higher organisms forms chlorophyll-protein complexes [40,41]. Hence, studying the phase behavior of disk-coil BCPs in confinement is essential to fully understand the self-assembled structure of chlorosome that may govern its photosynthetic performances.

In this paper, we studied the phase behavior of cylindrically confined disk-coil BCPs as functions of cylinder radius and the length of the coil. Concentric lamellar phases of alternating disk- and coil-rich layers arise due to the confinement by a coil-selective cylindrical wall. As the length of the coil portion increased, the number of disk-rich layers, enumerated from the surface to the core, was found to decrease. In addition, a significant difference was found in the molecular configuration of disks within different disk-rich layers, which shows the effect of curvature-induced frustrations that lead to deviation from the stacking behaviors found in bulk and a slab-confined system.

II. MOLECULAR MODEL AND COMPUTATIONAL DETAILS

We studied the phase behavior of disk-coil BCPs under cylindrical confinement by using molecular dynamics simulation. The disk block is composed of seven beads (monomers) forming a planar hexagon, and the coil block is composed of linearly connected N_c beads as shown in Fig. 1(a).

All neighboring beads are connected by stiff harmonic springs: $U(r) = \frac{1}{2}k(r - r_{\rm eq})^2$, where $r_{\rm eq} = 2^{1/6}\sigma$ is the equilibrium distance of the Lennard-Jones (LJ) potential described below, and $k = 1000\epsilon/\sigma^2$ is the spring constant of the harmonic potential. In order to maintain the planar shape of the disk block, three additional harmonic springs are introduced to three non-neighboring peripheral bead pairs as shown in Fig. 1(a) with $2k$ as the spring constant and $2r_{\rm eq}$ as the equilibrium distance. Cylindrical confinement is realized by a dense tube composed of immobile beads, which prevent the disk-coil molecules from escaping the cylindrical region.

In this simulation, four different types of beads are used to describe the interaction potential: (1) central bead of the disk, (2) peripheral beads of the disk, (3) beads of the coil, and (4) beads of the confining cylindrical wall. Beads of types i and j interact via truncated and shifted 12-6 LJ potential $U_{\rm LJ}^{ij}$, described in the equation below,

$$U_{\rm LJ}^{ij} = \begin{cases} 4\epsilon\chi_{ij}\left[\left(\frac{\sigma}{r}\right)^{12} - \left(\frac{\sigma}{r}\right)^{6} - \left(\frac{\sigma}{r_c^{ij}}\right)^{12} + \left(\frac{\sigma}{r_c^{ij}}\right)^{6}\right], & \text{if } r < r_c^{ij}, \\ 0, & \text{if } r > r_c^{ij}, \end{cases} \tag{1}$$

where ϵ and σ are the Lennard-Jones energy and distance parameters. Each $U_{\rm LJ}^{ij}$ is described by two additional parameters χ_{ij} and r_c^{ij}, which denote the interaction strength and the cutoff distance of the potential, respectively. For each (i, j) bead pair, values of χ_{ij} and r_c^{ij} are listed in Table I. All beads are of the same mass m.

Here, we give an overview of the interactions. The standard LJ potential ($\chi_{ij} = 1.0$ and $r_c^{ij} = 3.0\sigma$) is applied between two beads of the disk, whereas the stronger LJ potential ($\chi_{ij} = 3.0$ and $r_c^{ij} = 3.0\sigma$) is applied between the central beads of the disk to mimic the stacking nature of discotic molecules. Between the beads of the coil, we use the weakly

TABLE I. Parameters of interaction potential (χ_{ij} and r_c^{ij}) between different types of beads.

Bead i	Bead j	χ_{ij}	r_c^{ij}
Type 1	Type 1	3.0	3.0σ
Type 1 or 2	Type 2	1.0	3.0σ
Type 1 or 2	Type 3	1.0	$2^{1/6}\sigma$
Type 3	Type 3	0.05	3.0σ
Type 1 or 2	Type 4	1.0	$2^{1/6}\sigma$
Type 3	Type 4	0.1	3.0σ

attractive LJ potential ($\chi_{ij} = 0.05$ and $r_c^{ij} = 3.0\sigma$) to model relatively weak interaction of side chains as carried out in previous studies [17,18]. To model the amphiphilic nature of the disk-coil BCPs, we let disk and coil beads interact with purely repulsive Weeks-Chandler-Anderson potential ($\chi_{ij} = 1.0$ and $r_c^{ij} = 2^{1/6}\sigma$) [42]. Finally, the wall beads are modeled to prefer the coil beads over the disk beads by letting wall-coil and wall-disk interactions be weakly attractive and repulsive, respectively. Since beads of the confining cylindrical wall are immobile, no potential is required between beads of the wall.

Structural behaviors of disk-coil BCPs are sampled by molecular dynamics simulation using Large-Scale Atomic/Molecular Massively Parallel Simulator [43]. An isobaric-isothermal ensemble is used where the temperature and pressure are maintained at the target value by the Langevin thermostat and Berendsen barostat, respectively. Since the system is confined in a cylinder, the barostat is applied only to the axial direction (z) of the cylinder, hence, maintaining the x and y dimensions constant in Fig. 1(b). The Newtonian equation of motion is integrated using the standard velocity-Verlet algorithm with a time step of 0.01τ, where τ is the Lennard-Jones unit time $\sqrt{m\sigma^2/\epsilon}$. The damping timescales of the thermostat and barostat are 2.0τ and 100.0τ, respectively.

The simulation workflow goes as follows. The initial configuration of the system is randomly distributed disk-coil BCPs in a cylinder without considering the overlap between beads. The system is then relaxed using a core-softened LJ potential [44], described in the equation below, which prevents the system from blowing up

$$U_{cs}^{ij} = 4\lambda^2\epsilon\chi_{ij}\left\{\left[0.5(1-\lambda)^2+\left(\frac{r}{\sigma}\right)^6\right]^{-2}-\left[0.5(1-\lambda)^2+\left(\frac{r}{\sigma}\right)^6\right]^{-1}-\left[0.5(1-\lambda)^2+\left(\frac{r_c^{ij}}{\sigma}\right)^6\right]^{-2}+\left[0.5(1-\lambda)^2+\left(\frac{r_c^{ij}}{\sigma}\right)^6\right]^{-1}\right\}, \quad (2)$$

where λ is the activation parameter between 0 and 1. For $\lambda < 1$, $U(r)$ has no singularity at $r = 0$, and for $\lambda = 1$, $U(r)$ recovers the standard LJ potential. During relaxation steps, λ is slowly increased from 0 to 1 in NVT simulations for $5 \times 10^3\tau$ at $T = 2.0\epsilon/k_B$. After the relaxation step, to minimize the influence of metastability, the system is slowly cooled to a target temperature of $T = 1.3\epsilon/k_B$ for $1.6 \times 10^5\tau$. After reaching the target temperature, the system is equilibrated for $5 \times 10^4\tau$, which is long enough for the equilibration run as shown in Fig. S1 in the Supplemental Material [45], in the NPT ensemble at a target pressure of $P_z = 0.1\epsilon/\sigma^3$. All data are collected during a subsequent simulation run (production run as shown in Fig. S1 of the Supplemental Material [45]) of $5 \times 10^4\tau$ for every 100τ to calculate ensemble-averaged properties. Note that the final simulation condition $T = 1.3\epsilon/k_B$ and $P = 0.1\epsilon/\sigma^3$ is where disk-coil BCPs in bulk environment are stabilized with the phase separated lamellar structure without crystallized disks as shown in previous simulation studies [18]; see also Fig. S2 of the Supplemental Material for representative snapshots [45]. Finally, the number of molecules in each system is chosen so that equilibrated cylinder length is larger than 40σ to avoid finite size effects on the z direction of the simulation system. Details of the simulation conditions, including the number of coil beads N_c, cylinder diameter D, and the number of disk-coil BCPs N_{BCP}, can be found in Table SI of the Supplemental Material [45].

III. RESULTS AND DISCUSSIONS

In this paper, we study the phase behavior of cylindrically confined disk-coil BCPs. The equilibrium configuration here is concentric cylindrical lamellae composed of alternating disk-rich and coil-rich tubular bilayers as shown in Fig. 2(a) which is similar to the concentric lamellar phase of coil-coil BCPs confined within a cylinder from previous studies

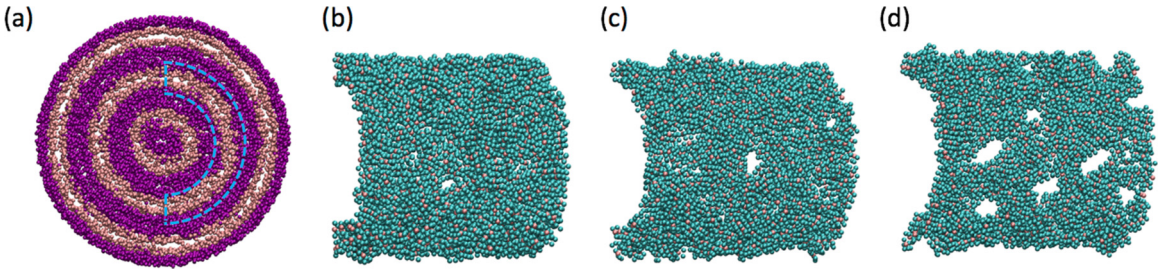

FIG. 2. (a) A snapshot of the self-assembled structure of disk-coil BCPs with $N_c = 3$ and $D = 58.90\sigma$, showing three alternating layered structures. The disk center and coil beads are represented as pink and purple beads, respectively. Peripheral beads of the disks are not shown to emphasize the bilayer structure of the disk-rich layers. (b)–(d) Snapshots of half-concentric lamella highlighted with a blue dashed line in (a) of disk-coil BCPs with (b) $N_c = 3$, $D = 58.90\sigma$, (c) $N_c = 4$, $D = 61.20\sigma$, and (d) $N_c = 5$, $D = 63.68\sigma$ where disk-center and disk periphery beads are represented as pink and blue beads, respectively. In (b)–(d), coil beads are removed for visual purpose.

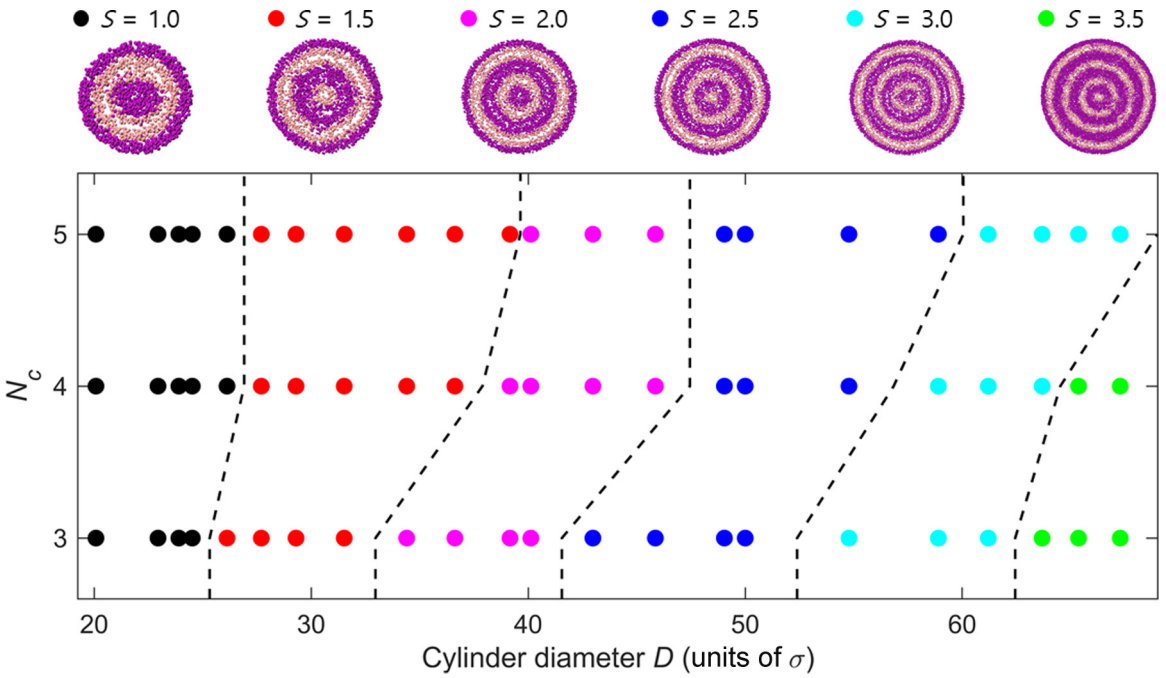

FIG. 3. Structures of disk-coil BCPs in cylindrical confinement as functions of the number of beads of coil N_c and the diameter of cylindrical wall D. Dots denote the simulation results, and dashed lines denote hypothetical boundaries. The inset figures are representative snapshots of each structure described by parameter S where the disk-center and coil beads are represented as pink and purple beads, respectively. Peripheral beads of disks are not shown to emphasize the bilayer structure of the disk-rich layers. Note that inset figures are not shown on the same length scale: Snapshots for larger S are obtained from simulations with larger D.

[26–31]. Similar to the bulk structure of disk-coil BCPs, concentric cylindrical disk-rich layers of disk-coil BCPs confined in a cylinder contain more pores composed of coil beads with increased N_c as shown in Fig. 2(b)–2(d). Since the confining wall prefers the coil block, the outermost layer is always coil rich. As a result, the system contains several concentric disk bilayers with either a coil-rich or a disk-rich cylinder core. We identify the structure of this system with the number of disk bilayers S formed within the cylinder. For example, if the system contains two disk bilayers with coil-rich innermost cores of the cylinder, S is 2.0, whereas if the system contains one disk bilayer with a disk-rich innermost core of the cylinder, S is 1.5; see Fig. 3.

As shown in Fig. 3, the structural behavior of cylindrically confined disk-coil BCPs can be described by two parameters: (1) N_c, the number of coil beads in a disk-coil BCP and (2) D, the diameter of the confining cylindrical wall. In general, disk-coil BCPs with larger N_c would exhibit larger bulk periodic lamellar spacing. In our system, lamellar spacing of bulk disk-coil BCPs of $N_c = 3$–5 are 8.82σ, 9.35σ, and 9.71σ, respectively, as shown in Fig. S2 of the Supplemental Material [45]. As a result, the system with a larger N_c tends to have fewer layers compared to the systems with smaller N_c. This is shown in Fig. 3 where the boundaries between structures move to larger values of D as N_c is increased.

The concentric cylindrical lamellar structure differs from bulk lamellar structure in that each layer experiences nonzero curvature, which gets smaller in the outer layers and vanishes in the limit of infinite diameter. Although disks prefer to be stacked in parallel due to strong center-center attractions, curvature introduces the spatial frustration to the stacked structure in the disk-rich layer. The hallmark of cylindrically confined disk-coil BCPs is this curvature-induced structural frustration on which we focus in this paper. To better address the curvature effects, we mainly analyze the systems of three disk bilayers ($S = 3.0$) and compare the spatial and orientational characteristics among the three disk-rich layers.

In Fig. 4, we plotted the local density distribution function of central beads of disks $P(r)$ as functions of r/D and the number of beads of coil N_c for $S = 3.0$, where r is the radial distance from the cylinder core. Let r_i denote the radial distance of the disk central bead of the ith BCP in a system composed of N_{BCP} disk-coil BCPs. $P(r)$ is calculated from the histogram of r_i with bin size $\Delta r = D/200$. To investigate the curvature effect of the distribution of disks in the system, we also simulated slab-confined disk-coil BCPs where the confining slabs are separated by distance D (See Fig. S3 of the Supplemental Material for more details of the slab-confined simulation [45]). $P(r)$ for slab-confined disk-coil BCPs is also plotted in Fig. 4 as a function of r/D, where r is the distance from the center of the two confining slabs. $P(r)$ is decreased with smaller values of r/D for all conditions of N_c for both cylinder- and slab-confined cases. Since the confining wall is composed of coil-attractive beads, coil beads are selectively attracted to the confining wall. As a result, the outermost layer of disk-coil lamellae has less fluctuation compared to inner layers; see Fig. S5 in the Supplemental Material [45]. In Fig. 4, this effect is expressed as sharp peaks in $P(r)$. Also, $P(r)$ decreases with increased N_c due to the formation of the pores of disk-coil BCPs with higher N_c as shown in Figs. 2 and S3 of the Supplemental Material [45] under both cylinder and slab confinements.

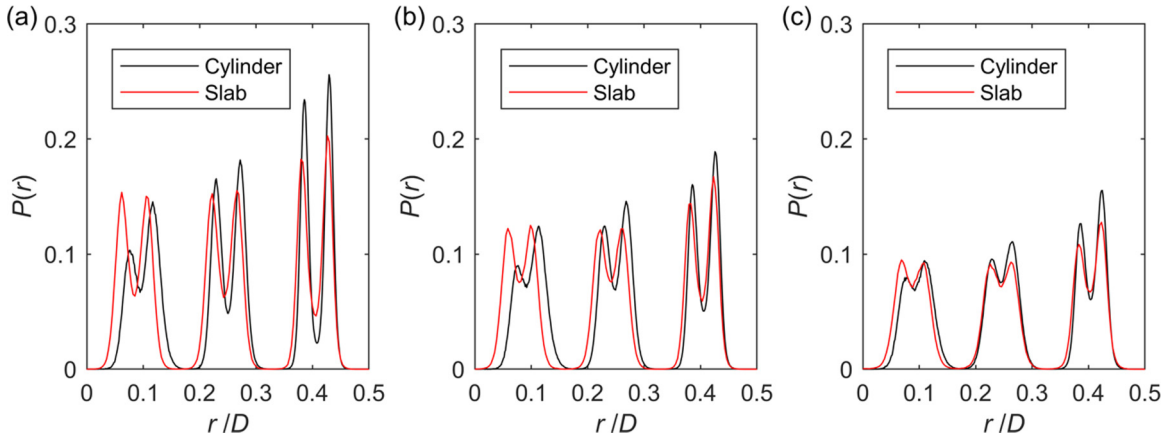

FIG. 4. Local density distribution function $P(r)$ (in units of σ^{-3}) of central beads of the disk for $S = 3.0$, acquired from simulations with (a) $N_c = 3,\ D = 58.90\sigma$, (b) $N_c = 4,\ D = 61.20\sigma$, and (c) $N_c = 5,\ D = 63.68\sigma$, plotted as a function of r/D where r is the radial distance from the cylinder core. Corresponding simulation results of slab-confined disk-coil BCPs are acquired under conditions from Fig. S3 of the Supplemental Material [45]. For the case of slab confinement, r and D denotes the distance from the center of the two confining slabs and the distance between slabs, respectively.

However, $P(r)$ of the cylinder- and slab-confined systems show notable differences in the inner layers that are not directly attached to the confining wall. Note that, as r/D decreased, the effect of the confining wall diminishes for both the cylinder- and the slab-confined systems whereas the curvature in the cylinder-confined system increased. Hence, the difference between the inner layers of the cylinder- and slab-confined systems highlights the effect of curvature on the structural behavior of disk-coil BCPs. In the slab-confined system, $P(r)$ of inner layers are symmetric in shape, i.e., the two sublayers are of equal height and shape. In addition, $P(r)$'s of inner layers approach that of bulk disk-coil BCPs (Fig. S4 of the Supplemental Material [45]), which implies that the effect of the confining wall is negligible in the inner layers. On the other hand, inner layers of cylinder-confined systems are asymmetric in shape, where $P(r)$ of the outer sublayer is higher than that of the inner sublayer. This is mainly due to the curvature-induced geometric frustration of the disk portions in BCPs: The curvature of the disk-rich domain leads the disks to be imperfectly stacked of which the effect is stronger in regions with larger curvature, i.e., inner layers. This effect especially manifests in the interlayer difference: Fig. 4 shows that peaks of $P(r)$ tend to be smaller and broader in inner layers, and Fig. S5 of the Supplemental Material shows that the disks in inner layers are more mobile than those in outer layers [45].

However, it should be noted that the static and dynamic characteristics in each sublayer are not perfectly described as a function of domain curvature. Figure S5 of the Supplemental Material [45] shows that the average displacement of disks follows a steplike trend where the disks in the outer sublayer show a larger position fluctuation than those in the inner sublayer. This is partially due to the curvature-induced asymmetric stretching of the coil portion in BCPs. Coils attached to the outer sublayer of disks are stretched toward the less curved region, whereas coils attached to the inner sublayer of disks are stretched toward the more curved region as shown in Fig. S6 of the Supplemental Material [45]. As a result, coils attached to the outer sublayer experience more free volume compared to coils attached to the inner sublayer. Therefore, the free energy of the system is minimized by balancing the free volume of coils from the asymmetric local density of disk-coil BCPs between inner and outer layers: see also the steplike variation of local volume and radius of gyration of coil portions of Table SII and SIII in the Supplemental Material [45].

For the systems with higher N_c, this asymmetry of the local density is further reduced due to the relaxation of coils through the pores of disk-rich layers. Figure S7 of the Supplemental Material [45] shows that in systems with larger N_c, the local density of coil beads in disk-rich domains is nonzero and increases with domain curvature, which implies that pore formation is facilitated in systems with larger N_c and larger curvature. This is reflected in Fig. 4 where the intralayer asymmetry in $P(r)$ is less severe in systems with larger N_c.

Now, we move on to analyze the effect of curvature and N_c on the orientational distribution of disks. Unlike coil-coil BCPs that do not have specific orientational preferences, disk-coil BCPs have a preferred direction of alignment due to the rigidity of disks. To quantify the orientational distribution of disks in a manner relevant to the symmetry of the cylindrical system, we construct an angular parameter θ for the ith BCP as follows. First, we define the "director vector" $\vec{v}_i$ normal to the disk plane, which is calculated from the averaged cross product of in-plane vectors of the ith disk: The cross products of different combinations of in-plane vectors are averaged to minimize the effect of the fluctuation of the disk shape. Note that in lamellar phases of disk-coil BCPs in bulk, the director vectors are oriented parallel to the lamellar plane where each disk is stacked to two adjacent disks to form a disk-rich domain [17]. In concentric lamellar phases of cylinder-confined systems, the normal vector of the lamellar plane should be replaced by the radial vector from the cylinder axis $\vec{r}_i = (x_i - x_0, y_i - y_0, 0)$, where x_0 and y_0 denote the x and y coordinates of the axis, respectively. Then, the angle between the director and the radial vectors is calculated as $\theta_i = \arccos\left(\frac{\vec{v}_i \cdot \vec{r}_i}{|\vec{v}_i||\vec{r}_i|}\right)$. The orientational distribution function $G(r, \theta)$ is constructed from the

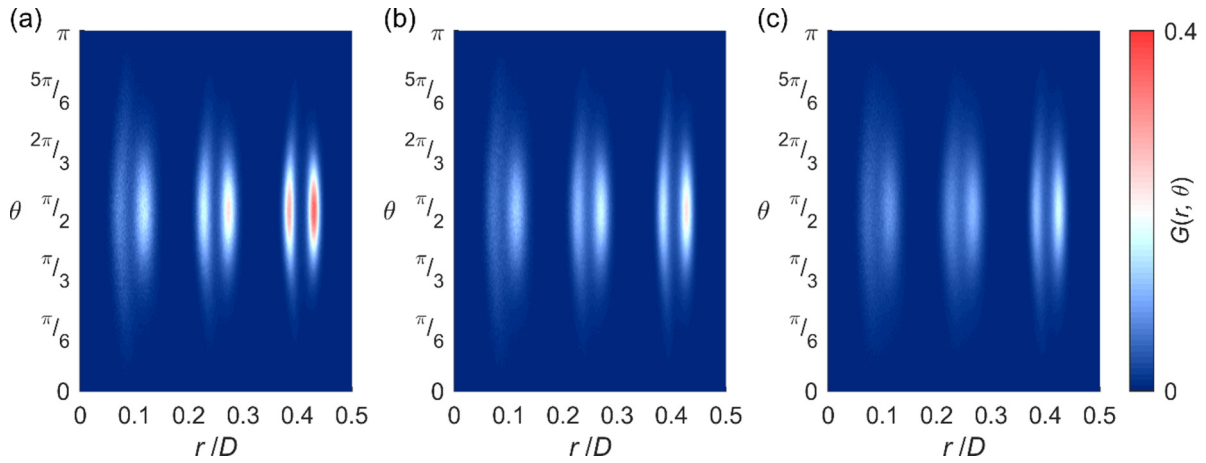

FIG. 5. The orientational distribution function $G(r,\theta)$ of disks for $S = 3.0$, acquired from simulations with (a) $N_c = 3$, $D = 58.90\sigma$, (b) $N_c = 4$, $D = 61.20\sigma$, and (c) $N_c = 5$, $D = 63.68\sigma$, plotted as a function of r/D and θ, where θ is the relative angle between the director vector of the disk and the radial vector from the cylinder axis.

bivariate histogram of (r_i, θ_i) with bin sizes $D/200$ and $\pi/180$, respectively,

$$G(r,\theta) = \left\langle \lim_{\Delta r, \Delta\theta \to 0} \frac{\sum_i \delta(r - r_i)\delta(\theta - \theta_i)}{2\pi r L\, \Delta r\, \Delta\theta} \right\rangle, \tag{3}$$

which is normalized to satisfy $\int_0^\pi G(r,\theta)d\theta = P(r)$, i.e., integration over θ yields the local density distribution function $P(r)$ in Fig. 4.

Figure 5 shows $G(r,\theta)$ acquired from the same systems as in Fig. 4. Note that the orientational distribution of all layers is symmetric with respect to the peak at $\theta = \pi/2$. This implies that director vectors of disks in concentric lamellar disk-coil BCPs also prefer to be oriented perpendicular to the radial vector. The peak value of $G(r,\theta)$ is higher in the outer layers and is decreased in inner layers with the same asymmetry between sublayers as is in $P(r)$ of Fig. 4. Also, the variance of θ distribution is much larger in inner layers than in outer layers, where $G(r,\theta)$ of the innermost sublayer shows significantly longer tail in θ direction compared to outer sublayers, especially in systems with smaller N_c. This highlights the effect of curvature on the orientational order within disk-rich layers: In the course of balancing entropic cost due to asymmetric free volume between sublayers, the orientational order due to stacked disk is decreased.

In addition, a comparison between $G(r,\theta)$ of different coil lengths implies that pore formation provides another mechanism to relax the curvature-induced free volume asymmetry. It is observed that in systems with larger N_c, the θ distribution gets more broadened, and the asymmetry within the bilayers is reduced. This is due to the increased porosity in systems with longer coils (see Fig. 2 and Fig. S7 of the Supplemental Material [45]); coil portions of pore-exposed BCPs are stretched toward in-plane directions rather than radial directions, which leads their disk portions to be oriented in different directions. Furthermore, pores provide entropic gain due to the increased free volume of coil portions, hence, the enthalpic cost due to misaligned disk portions is compensated in systems with longer coils.

IV. CONCLUSION

In this article, we studied the phase behavior and the structural characteristics of disk-coil BCPs confined in a coil-selective cylindrical wall using molecular dynamics simulations where we acquired concentric lamellar structures with alternating disk- and coil-rich bilayers. Identifying the structure with respect to the number of disk-rich layers, we observed the structural evolution of the system as functions of the cylinder diameter D and the number of coil beads N_c. The hallmark of this system is the curvature-induced structural frustration, which leads to deviation of spatial and orientational properties from those of bulk or slab-confined systems. The spatial characteristics of the system were studied by means of local density distribution function $P(r)$. Unlike the inner layers of slab-confined systems that approach bulk structures, the inner layers of cylinder-confined systems show strongly asymmetric $P(r)$ peaks: The large curvature near the cylinder core leads to asymmetric local density of coil portions attached to inner layers, and this entropic cost is compensated by balancing their free volume. This trend is also observed in the orientational distribution function $G(r,\theta)$, which shows that the angle between the director vector of disks and the cylinder core is more broadly distributed in the inner layers than in the outer layers. One interesting point to note is that in systems with larger N_c, both $P(r)$ and $G(r,\theta)$ show reduced asymmetry in inner layers. Disk-coil BCPs with longer coils lead to increased porosity in the disk-rich layers which implies that pore provides another mechanism to relax the curvature-induced frustrations in self-assembled structure of disk-coil BCPs within a cylinder.

The study of cylinder-confined disk-coil BCPs has implications on the self-assembly of Bchl molecules into chlorosome, the light-harvesting antennae complex of phototrophic bacteria, which is generally believed to be guided by its confining membranes. Considering the cylindrical or ellipsoidal

shape of the chlorosome envelope, the result of this paper is directly linked to the structural study on the self-assembled structure of chlorophyll molecules. By using coarse-grained molecules that mimic the disk-coil motif, our paper on the curvature-induced structural frustration of disks opens up the possibility to understand the complex packing structure of Bchl molecules, which often experience asymmetric intermolecular interactions within the chlorosome. For future direction, there is additional room for more interesting and realistic modeling by introducing asymmetric stacking interaction between peripheral beads of the disk using the coarse-grained or all-atomic simulation model. We plan to study more sophisticated systems with asymmetric stacking interactions, which goes along with a comparison to the experimental study on the self-assembly of synthetic disk-coil BCPs.

ACKNOWLEDGMENTS

This research was supported by National Research Foundation of Korea (NRF) Grant funded by Korean Government through the Ministry of Science, ICT, and Future Planning (MSIP) (Grant No. NRF-2015R1A5A1036133), and NRF Grant funded by Korean Government (Grant No. NRF-2017R1A6A3A04009006).

[1] F. S. Bates and G. H. Fredrickson, Phys. Today **52**(2), 32 (2000).
[2] C. M. Bates and F. S. Bates, Macromolecules **50**, 3 (2016).
[3] M. P. Stoykovich, M. Müller, S. O. Kim, H. H. Solak, E. W. Edwards, J. J. de Pablo, and P. F. Nealey, Science **308**, 1442 (2005).
[4] M. P. Stoykovich, H. Kang, K. C. Daoulas, G. Liu, C.-C. Liu, J. J. de Pablo, M. Müller, and P. F. Nealey, ACS Nano **1**, 168 (2007).
[5] J. Bang, U. Jeong, D. Y. Ryu, T. P. Russell, and C. J. Hawker, Adv. Mater. **21**, 4769 (2009).
[6] R. A. Segalman, Mater. Sci. Eng. R: Rep. **48**, 191 (2005).
[7] H. Shen and A. Eisenberg, J. Phys. Chem. B **103**, 9473 (1999).
[8] F. S. Bates and G. H. Fredrickson, Annu. Rev. Phys. Chem. **41**, 525 (1990).
[9] L. Leibler, Macromolecules **13**, 1602 (1980).
[10] M. W. Matsen and M. Schick, Phys. Rev. Lett. **72**, 2660 (1994).
[11] J. T. Chen, E. L. Thomas, C. K. Ober, and G.-P. Mao, Science **273**, 343 (1996).
[12] J. T. Chen, E. L. Thomas, C. K. Ober, and S. S. Hwang, Macromolecules **28**, 1688 (1995).
[13] M. Lee, B.-K. Cho, and W.-C. Zin, Chem. Rev. **101**, 3869 (2001).
[14] E. A. Minich, A. P. Nowak, T. J. Deming, and D. J. Pochan, Polymer **45**, 1951 (2004).
[15] A. Halperin, Macromolecules **23**, 2724 (1990).
[16] Y. Kim and A. Alexander-Katz, J. Chem. Phys. **132**, 174901 (2010).
[17] Y. J. Kim and A. Alexander-Katz, J. Chem. Phys. **135**, 024902 (2011).
[18] Y. J. Kim, E. Ha, and A. Alexander-Katz, Macromolecules **44**, 7016 (2011).
[19] A. N. Semenov, Mol. Cryst. Liq. Cryst. **209**, 191 (1991).
[20] N. Sary, R. Mezzenga, C. Brochon, G. Hadziioannou, and J. Ruokolainen, Macromolecules **40**, 3277 (2007).
[21] A. Halperin, Europhys. Lett. **10**, 549 (1989).
[22] S. O. Kim, H. H. Solak, M. P. Stoykovich, N. J. Ferrier, J. J. de Pablo, and P. F. Nealey, Nature (London) **424**, 411 (2003).
[23] J. N. L. Albert and T. H. Epps III, Mater. Today **13**, 24 (2010).
[24] G. Krausch and R. Magerle, Adv. Mater. **14**, 1579 (2002).
[25] B. Yu, P. Sun, T. Chen, Q. Jin, D. Ding, B. Li, and A.-C. Shi, Phys. Rev. Lett. **96**, 138306 (2006).
[26] A.-C. Shi and B. Li, Soft Matter **9**, 1398 (2013).
[27] B. Yu, P. Sun, T. Chen, Q. Jin, D. Ding, B. Li, and A.-C. Shi, J. Chem. Phys. **127**, 114906 (2007).
[28] W. Li, R. A. Wickham, and R. A. Garbary, Macromolecules **39**, 806 (2006).
[29] H. Xiang, K. Shin, T. Kim, S. I. Moon, T. J. McCarthy, and T. P. Russell, Macromolecules **37**, 5660 (2004).
[30] G. J. A. Sevink, A. V. Zvelindovsky, J. G. E. M. Fraaije and H. P. Huinink, J. Chem. Phys. **115**, 8226 (2001).
[31] Y. Sun, M. Steinhart, D. Zschech, R. Adhikari, G. H. Michler, and U. Gösele, Macromol. Rapid Commun. **26**, 369 (2005).
[32] P. Chen, H. Liang, and A.-C. Shi, Macromolecules **41**, 8938 (2008).
[33] L. Li, K. Matsunaga, J. Zhu, T. Higuchi, H. Yabu, M. Shimomura, H. Jinnai, R. C. Hayward, and T. P. Russell, Macromolecules **43**, 7807 (2010).
[34] J.-H. Huang, J.-J. Wu, and X.-W. Huang, RSC Adv. **6**, 100559 (2016).
[35] T. S. Balaban, Acc. Chem. Res. **38**, 612 (2005).
[36] T. S. Balaban, H. Tamiaki, and A. R. Holzwarth, Top. Curr. Chem. **258**, 1 (2005).
[37] J. M. Linnanto and J. E. I. Korppi-Tommola, Photosynth. Res. **96**, 227 (2008).
[38] T. Jochum, C. M. Reddy, A. Eichhöfer, G. Buth, J. Szmytkowski, H. Kalt, D. Moss, and T. S. Balaban, Proc. Natl. Acad. Sci. USA **105**, 12736 (2008).
[39] A. Egawa, T. Fujiwara, T. Mizoguchi, Y. Kakitani, Y. Koyama, and H. Akutsu, Proc. Natl. Acad. Sci. USA **104**, 790 (2007).
[40] J. Pšenčík, T. P. Ikonen, P. Laurinmäki, M. C. Merckel, S. J. Butcher, R. E. Serimaa, and R. Tuma, Biophys. J. **87**, 1165 (2004).
[41] W. Kühlbrandt, Nature (London) **307**, 478 (1984).
[42] J. D. Weeks, D. Chandler, and H. C. Andersen, J. Chem. Phys. **54**, 5237 (1971).
[43] S. Plimpton, J. Comput. Phys. **117**, 1 (1995).
[44] T. C. Beutler, A. E. Mark, R. C. van Schaik, P. R. Gerber, and W. F. van Gunsteren, Chem. Phys. Lett. **222**, 529 (1994).
[45] See Supplemental Material at http://link.aps.org/supplemental/10.1103/PhysRevE.100.052502 for computational details, bulk simulation results, and supporting data for asymmetric coil stretching.